

Identifying Spurious Correlations using Counterfactual Alignment

Joseph Paul Cohen*
Stanford University

joseph@josephpcohen.com

Louis Blankemeier
Stanford University

Akshay Chaudhari
Stanford University

Abstract

Models driven by spurious correlations often yield poor generalization performance. We propose the counterfactual alignment method to detect and explore spurious correlations of black box classifiers. Counterfactual images generated with respect to one classifier can be input into other classifiers to see if they also induce changes in the outputs of these classifiers. The relationship between these responses can be quantified and used to identify specific instances where a spurious correlation exists as well as compute aggregate statistics over a dataset. Our work demonstrates the ability to detect spurious correlations in face attribute classifiers. This is validated by observing intuitive trends in a face attribute classifier as well as fabricating spurious correlations and detecting their presence, both visually and quantitatively. Further, utilizing the CF alignment method, we demonstrate that we can rectify spurious correlations identified in classifiers.

1. Introduction

Challenges related to neural network generalization and fairness often arise due to covariate shift [19] and shortcut learning [10]. Shortcut learning can lead to models making decisions based on factors not aligned with expectations of the model creator. These powerful models (vision models in this work) leverage a wide array of features and relationships, which may inadvertently incorporate undesired, spurious correlations. These spurious relationships may stem from sample bias (e.g., predicting cows when cows are observed on grass but not on a beach) or may be inherent to the class definition (e.g., predicting cows when an animal has four legs) [6].

Our primary goal is to ensure that models make predictions without relying on spurious correlates, a concept coined as “right for the right reasons” [25]. This means that the features employed for prediction align with expectations of the model creator, rather than features which are spu-

riously correlated with the target label. Models driven by such spurious correlations often yield poor generalization performance [6, 10]. Consequently, it is crucial to develop methods for uncovering and correcting these unwanted correlations.

Our objective is to understand black-box classifiers, such as pre-trained models, as this is a common use case encountered by practitioners. In this analysis, we utilize counterfactual (CF) images, synthetic images simulating a change in the class label of an image [35]. These synthetic images have features modified such that the prediction of the classifier changes. We can then view the synthetic images to understand the reasons that a prediction was made.

Specifically, we are interested in CF images that are directly generated using the gradients of a classifier [3, 8, 12]. Generating CF images with respect to a classifier is rooted in similar logic to that of crafting adversarial examples. However, the key distinction lies in the constraint that CF images remain within the data manifold of plausible images. The latent space of an autoencoder provides such data manifold. This approach enables us to study the specific features used by a given classifier on a particular input. By keeping the classifier and autoencoder independent, different classifiers can be analysed using a singular fixed autoencoder as a reference point.

The task of interpreting these CF images presents new challenges of scale. Spurious correlations may only exist in a handful of samples where rare features occur together. Locating these samples requires investigating the features used for each prediction, which can be automated using the approaches we present in this study.

The approach we take is to generate CF images for the positive predictions of a classifier over an entire dataset and study the resulting CF images using a collection of different classifiers, which we refer to as downstream classifiers, to observe what outputs are impacted. If the CF images generated for one classifier also change the predictions of other classifiers, we can conclude there is shared feature usage. This shared feature usage can prompt us to investigate unexpected relationships. The relative change metric (Eq. 3) can be used to identify spurious correlations which may oc-

¹Work done prior to joining Amazon

cur for a specific example or to identify trends over an entire dataset. We study face attribute classification, recognizing its advantage in allowing visual verification by readers.

Overall, given the problem setting of spurious correlations, the contributions of this work include:

- We propose CF alignment to reason about the feature relationships between classifiers. This approach allows for both aggregate quantification and targeted querying of models to identify instances where incorrect reasoning leads to a prediction.
- Our work demonstrates the ability to detect spurious correlations in face attribute classifiers. This is validated by observing intuitive trends in a face attribute classifier as well as inducing spurious correlations and then detecting their presence, both visually and quantitatively.
- Utilizing the CF alignment method, we demonstrate that we can rectify spurious correlations identified in classifiers. Experimental results show a bias reduction in 10 out of 12 classifiers.

2. Related Work

Counterfactual (CF) generation can be done in a variety of ways [35]. Classifier specific approaches generally perturb a latent space representation guided by a classifier. Some methods use the gradient of a classifier to guide movement in the latent space by computing the gradient directly [8] or defining a loss that is optimized [3, 12]. Another classifier based approach is to train a model that predicts, using training examples, where to walk in the latent space to change the classifier’s prediction [28]. This has the benefit of working with classifiers that are not differentiable. Another approach is conditional generation which doesn’t use a classifier and instead generates images based on a conditioning variable. This conditioning can be a label [4, 5, 11, 18, 27, 28, 31] or text [7] or by manually adjusting the latent representation [29]. Conditional generation learns a representation from the data and does not capture the exact features utilized by a classifier, as the gradient based methods do.

Several methods exist for studying neural network based classifiers to understand the features they use. Early approaches include gradient based attribute maps (aka saliency heatmaps) that could be overlaid on the image [30]. This was extended to capture more caveats of neural network reasoning [32, 33] but these methods still only generate heatmap explanations. Other work focuses on leveraging occlusions to identify discrete image regions [23]. Other work inspects individual neural network neurons to identify where class information was propagating using linear probing [1] and manual identification [20, 21]. Additional methods focus on concepts represented by layer activations and identifying images that share these representations [14]. Another approach [2] generates synthetic images using hu-

man annotators such that the images have known feature similarity (e.g. a face with all features held constant except for skin color). These images are then used to identify spurious correlations between attributes.

3. Alignment Methodology

This work proposes the CF alignment approach as described in Fig. 1. For this approach, we generate counterfactuals using Latent Shift [8]. This approach requires an encoder/decoder model $D(E(x))$ where E is the encoder and D is the decoder, and a classifier f which predicts a target y as follows: $y = f(x)$. The autoencoder and the classifier are trained independently without specific requirements except for being differentiable and operating on the same data domain. To compute a counterfactual, an input image x is encoded using $E(x)$, to produce a latent representation z . Perturbations of the latent space are computed for a base classifier f_b in Eq. 1 which is then used to produce λ -shifted samples as shown in Eq. 2. λ is determined using an iterative search where the value is decreased in steps until the classifier’s prediction is reduced by 0.6 or begins to increase.

$$z_\lambda = z - \lambda \frac{\partial f_b(D(z))}{\partial z} \quad (1) \quad x'_\lambda = D(z_\lambda) \quad (2)$$

These counterfactual samples can then be input into downstream classifiers that predict various attributes (e.g. f_1, f_2) and observe how their predictions change. Relative change (Eq. 3) allows us to quantify the relationship between a base and downstream classifier, similar to correlation, but accounts for the magnitude of the change. In our experiments, we found correlation would produce false positives when there was only a slight change in the prediction of f_1 compared to the base classifier f_b .

$$\frac{f_1(D(z_\lambda)) - f_1(D(z_0))}{f_b(D(z_\lambda)) - f_b(D(z_0))} \quad (3)$$

4. Experiments

The experiments in this work are performed on the CelebA dataset [17] that contains over 200k celebrity images with 40 facial attribute labels per image. The resolution of the images is 1024×1024 .

The pre-trained face classifiers used in this work are sourced from [34]. They were trained on the CelebA dataset [17] to predict 40 different facial attributes on images of dimensions 224×224 . We chose this model because it has good performance, is publicly available, and was implemented in PyTorch.

We leverage the VQ-GAN autoencoder from [9] trained on the FacesHQ dataset, which combines the CelebA dataset [17] and the Flickr-Faces-HQ (FFHQ) dataset [13]. The resolution of this model is 256×256 .

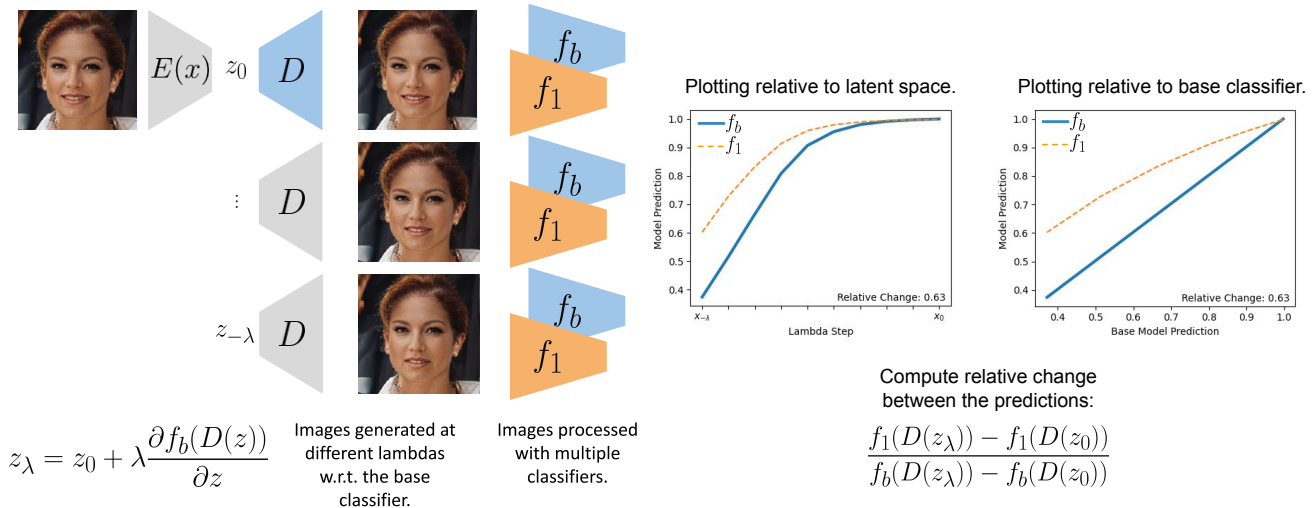


Figure 1. Overview of the alignment methodology. An image is encoded, reconstructed, and then processed by a classifier. The counterfactual is generated by subtracting the gradient of the classifier output w.r.t. the latent representation. The resulting representation is reconstructed back into an image. The reconstructed images are processed with multiple classifiers and the classifier outputs can be plotted side by side to study their alignment. The base model value can be used as the x-axis to more easily compare it to the predictions of another classifier. The output changes can be quantified and compared using relative change.

The Captum library [15] is utilized for baseline attribution methods. PyTorch [22] is used for efficient tensor computation and automatic differentiation. The source code and model weights for all experiments will be released publicly online*.

4.1. Aggregate statistics over a dataset

Viewing aggregate CF alignment statistics over a dataset can be useful when investigating a model for bias or spurious correlations. The average relative change between pairs of classifiers for 400 samples per class is shown in Fig. 2a. Figures 2b and 2c show correlations between classifier predictions and the ground truth training labels. Only an interesting subset of classifiers are shown in this figure for clarity, with the full CF alignment matrix in Appendix Fig. 9.

We draw the readers attention to the example relationship between *male* and *big_nose* in red, which is high in both classifier prediction and ground truth labels but very low using CF alignment. This indicates that while the attributes (labels) are correlated, the *male* classifier does not largely use *big_nose* as a feature to predict *male* - an expected insight that is verified. A similar insight is found for the class of *mouth_slightly_open*, which has a relatively strong relationship with *smiling*.

We also observe many non-symmetric relationships such as *male* and *wearing_lipstick* in green, as well as *young* and *attractive*. These are also intuitive relationships that we

would expect the classifiers to learn. The *male* classifier likely uses lipstick as a feature to reduce the likelihood that the image contains a *male* subject (high inverse correlation in Fig. 2c), while the *wearing_lipstick* classifier would be more focused on the color of the lips. Overall, these results help qualitatively depict that counterfactual reasoning can provide model introspection in a manner that is consistent with human reasoning.

4.2. Studying specific examples

Using the aggregate analysis from §4.1 as a guide, classifiers can be selected to investigate undesired relationships. We will first select a sample which contains an inverse relationship between a base classifier for *male* and downstream classifier for *heavy_makeup* in Fig. 3a. Visually, we can see makeup and lipstick in the CF image and the predictions increase as expected in the classifiers for *heavy_makeup*, *wearing_lipstick*, and *no_beard*. Similarly, there is a decrease in the classifier for *goatee*. These appear reasonable and provide insight about the features used for prediction. Exploring the more subjective base classifier label *attractive* in Fig. 3b we observe *big_nose* and *bags_under_eyes* increase, which can depict human preferences and biases in determining an *attractive* face.

4.3. Comparison with saliency maps

Saliency maps for feature attribution could potentially be used to perform a similar analysis by looking at relationships between their generated heatmaps. Here, we present

*<https://github.com/ieee8023/latentshift>

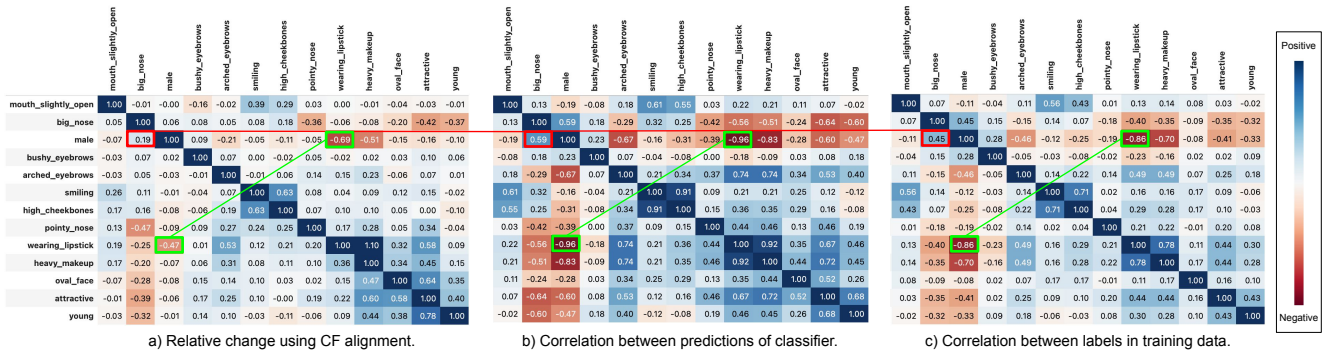


Figure 2. Relationships between face attribute classifiers as measured by CF-induced relative changes (left), classifier predictions (middle) and training data labels (right). In (a), base classifiers are along the rows and downstream classifiers are along the columns. Comparing (a) to (b) and (c), shows that many relationships reflected in the CF outputs are preserved from correlations in the training data. The non-symmetric relationship between *male* and *wearing_lipstick*, highlighted in green, reflects expected interactions between the two face attribute classifiers. The relationship between *male* and *big_nose*, highlighted in red, is strong in both the classifier predictions and ground truth labels but low in CF alignment, indicating that although correlated, these features aren't exploited by the classifier.

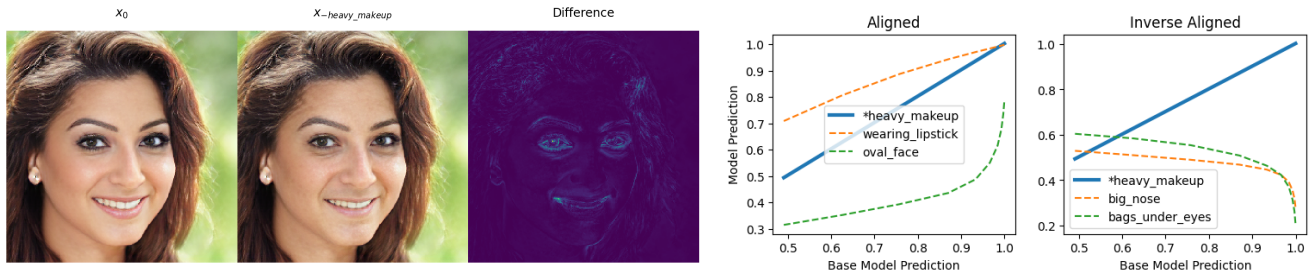
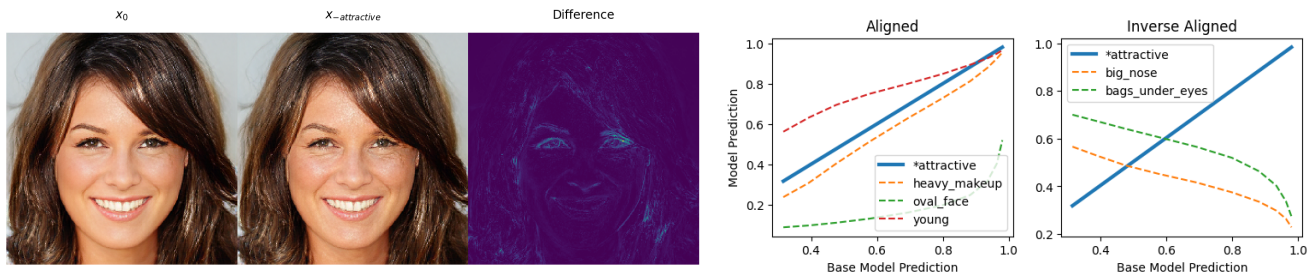
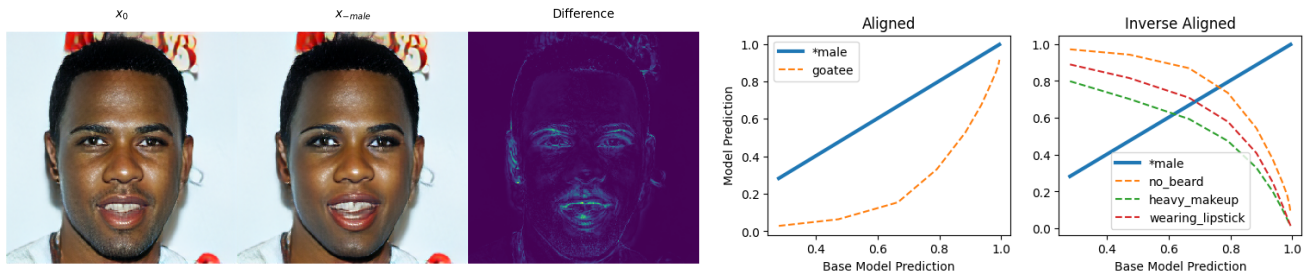


Figure 3. Examples of alignment for specific samples showing the visual counterfactual changes as well as other classifiers with aligned and inverse aligned relationships.

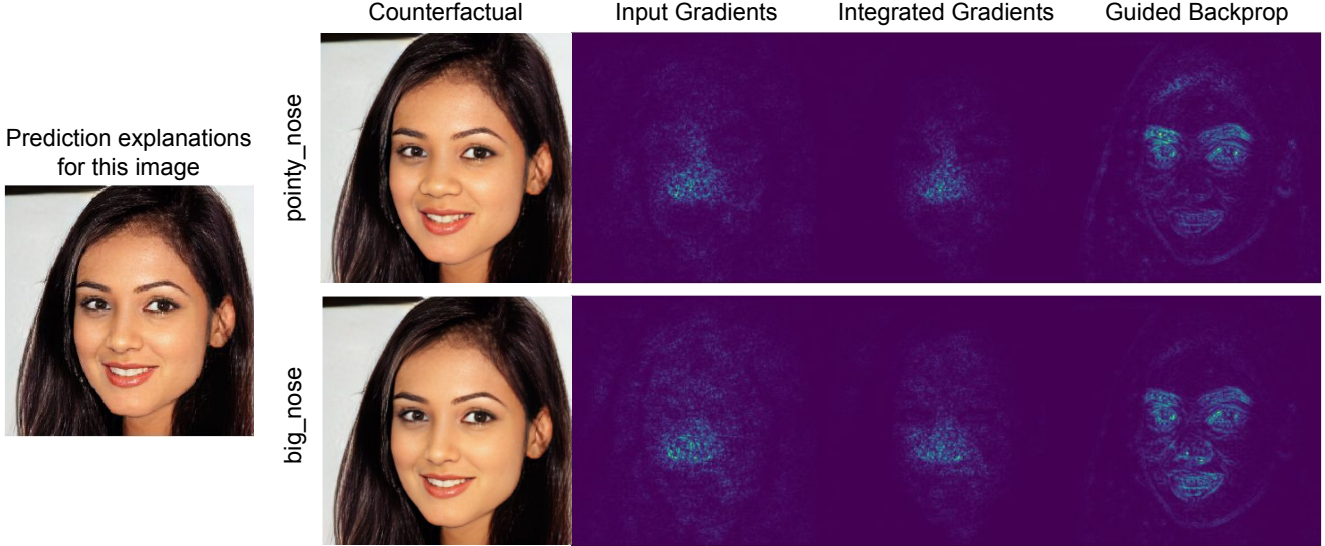


Figure 4. Example of saliency maps failing to provide meaningful localization when the concepts overlap with each other. Here, saliency map methods localize around the nose which doesn’t provide the ability to distinguish between a big or pointy nose prediction.

an example that demonstrates their limitation. The attribution methods input gradients, integrated gradients [33], and guided backprop [32] are used to explain the classifier predictions of *pointy_nose* and *big_nose*. In Fig. 4 the salient areas for *pointy_nose* and *big_nose* are the same and cannot be disambiguated. Comparing these heatmaps would yield a high similarity but we observe in Fig. 2 that these two classifiers have an inverse relationship. Using CF alignment, we can gain a deeper understanding of what features the model is using and better reason about why the decision was made.

4.4. Validation by inducing spurious correlations

In order to further verify the CF alignment approach, we construct a classifier with a known spurious correlation and then demonstrate that this bias is observable in the CF alignment plot. A spurious correlation can be induced in the classifier by composing classifiers:

$$f_{biased}(x) = f_{smiling}(x) + 0.3f_{arched_eyebrows}(x) \quad (4)$$

The CF alignment plot for the base *smiling* classifier predictions in Fig. 5a show that *arched_eyebrows* does not change and we can confirm this in the CF image. The resulting biased classifier can be observed using the *arched_eyebrows* features in Fig. 5b both visually as well as in the CF alignment plot. The CF alignment plot shows that the prediction of *arched_eyebrows* now changes and is aligned with *smiling*.

4.5. Rectifying bias by composing classifiers

This section demonstrates the use of CF alignment to fix model bias in classifiers. We can reuse the relative change

between model predictions as a loss function that can be minimized.

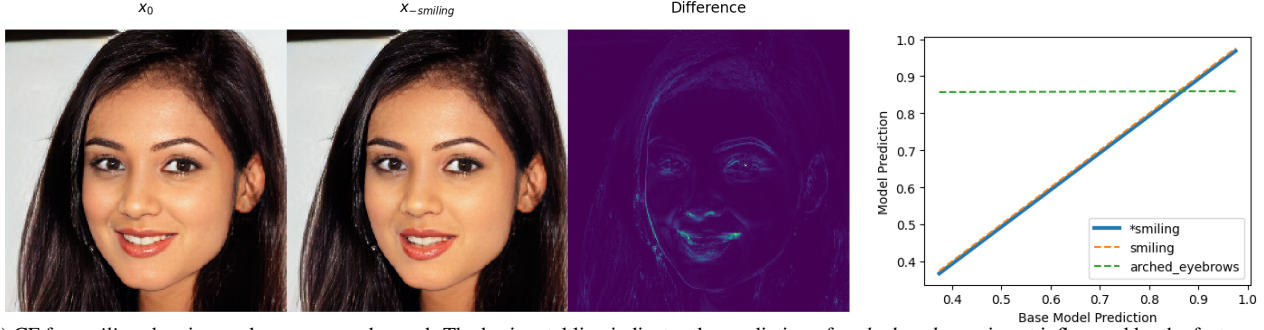
Correcting model bias and spurious correlations is an active area of research. Approaches include averaging model weights [36] or methods of invariant optimization [16, 24, 26, 37]. Composing classifiers can change their response to specific samples that contain relevant features as shown in §4.4. By using this additive composition approach we avoid the variance of model training which makes it easy and reproducible to perform experiments.

First, we demonstrate a single example of correcting bias. In Fig. 6, the CF image and CF alignment plot for the *heavy_makeup* base classifier show unexpected reductions in lip size. Composing the model with the *big_lips* classifier using a negative coefficient causes the classifier to lower any feature change focused on the lips as this would increase the prediction of the composed classifier (where the goal of the CF is to decrease it). We can also visually observe other features that change, such as skin color, bushy eyebrows, and the amount that the mouth is open.

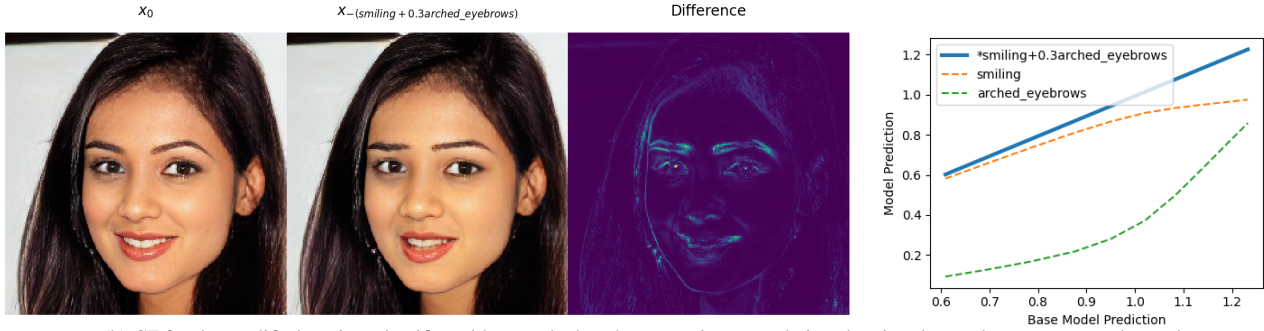
Next, this unbiasing is scaled up to a larger number of samples and classifiers. A collection of classifiers that contain varying spurious relationships to a *big_nose* base classifier (shown in Fig. 7a) are modified to remove their bias until their relative change is as close to 0 as possible. This experiment is performed with a train, validation, and hold out test set in order to demonstrate the generalization of this unbiasing process to unseen data.

The classifiers are modified using a single coefficient (β) such that the resulting classifier is

$$f'_{target}(x) = f_{target}(x) + \beta f_{big_nose}(x) \quad (5)$$



(a) CF for *smiling* showing eyebrows are unchanged. The horizontal line indicates the prediction of *arched_eyebrows* is not influenced by the features used for *smiling* in this image.



(b) CF for the modified *smiling* classifier with an arched eyebrow spurious correlation showing that eyebrows are now changed.

Figure 5. Example of detecting a spurious correlation in a biased classifier. The classifier is biased with arched eyebrows and this is observed in the alignment plot as well as in the counterfactual image. In order to decrease the prediction of the (now biased) classifier, the CF image can remove the arched eyebrows as well.

The optimization to compute β is performed using a pseudo gradient descent where the gradient is approximated by the mean relative change between the target classifier and the *big_nose* classifier. By subtracting the relative change from β , scaled by a learning rate, the relative change (ψ) with that classifier will be reduced. All together our training objective (including momentum) is

$$\beta_n = 0.001\psi(f_{target}, f_{big_nose}) + 0.1\beta_{n-1} \quad (6)$$

We find that using small minibatches of 10 samples works well because the computation time for each CF can take over 1 second on a GPU. Additionally, training with samples which induce a small change in the base classifier during the CF generation process can be challenging. As the classifiers are modified, this base change is reduced, which causes the relative change to become more erratic and prevents the optimization from converging. To prevent this, we use samples with a base change > 0.6 .

The resulting training metrics in Fig. 7 show model biases being summarized and minimized similar to a differentiable training loss. We observe a bias generalization gap between the train, valid, and test sets, indicating some degree of overfitting. Early stopping (red vertical line) is used on the validation set to determine the optimal param-

eters. We use momentum during training to average over the noise. The resulting reduction in bias is shown in Fig 7b. All biases are considerably reduced except for *attractive* and *big_nose*, which could be the result of overlapping features used by both classifiers that cannot be changed.

5. Limitations

There are limitations and challenges to CF generation [35] where bias can also exist in the CF generation method. Furthermore, although we are optimistic that our method will generalize to additional domains, we focus our current analysis on face attribute classification. Although we do not demonstrate the generalizability of our method to additional domains, using face attribute classification is a deliberate choice enabling qualitative evaluation, in addition to our quantitative evaluation. Additionally, since CF generation relies on a separate autoencoder, improving the representational capability of the autoencoder may improve the fidelity of the CF generation.

6. Conclusion

In this work we propose the counterfactual (CF) alignment approach to reason about the feature relationships in classi-



(a) As makeup is removed from the face, the lip size also shrinks.



(b) The lip size remains the same as the makeup is removed.

Figure 6. An example of a *big_lips* spurious correlation being corrected for the *heavy_makeup* classifier.

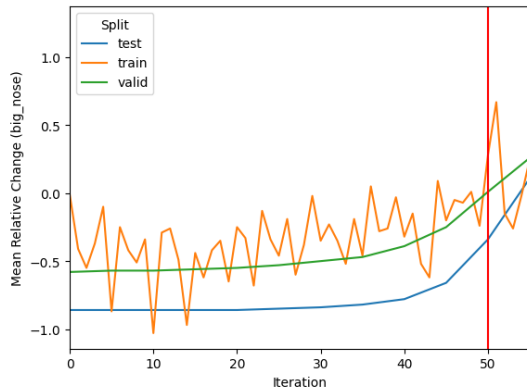


Figure 7. Training curves showing mean relative change during the optimization of a classifier with respect to the *big_nose* classifier during each iteration. The red vertical line is the early stopping point based on the validation set. This demonstrates how bias can be quantified and corrected using CF alignment.

fiers in aggregate statistics, to locate specific examples with spurious correlations, and propose strategies to mitigate the effect of spurious correlations. These claims are supported with an analysis of face attribute classifiers that identify many expected and unexpected spurious correlations such as *attractive* with *heavy_makeup* and *heavy_makeup* with

big_nose. The validity of the CF alignment method is confirmed by inducing and quantifying spurious correlations via additive composition. We then explore rectifying classifiers based on observed spurious correlations. Overall, the proposed approach may serve as an end-to-end or human-in-the-loop system to automatically detect, quantify, and correct spurious correlations for image classification tasks that lead to biased classifier outputs.

7. Acknowledgments

We would like to thank Stanford University and the Stanford Research Computing Center for providing computational resources and support that contributed to these research results.

References

- [1] Guillaume Alain and Yoshua Bengio. Understanding intermediate layers using linear classifier probes. *International Conference on Learning Representations*, 2016. 2
- [2] Guha Balakrishnan, Yuanjun Xiong, Wei Xia, and Pietro Perona. Towards Causal Benchmarking of Bias in Face Analysis Algorithms. In *Computer Vision and Pattern Recognition*, 2021. 2
- [3] Rachana Balasubramanian, Samuel Sharpe, Brian Barr, Jason Wittenbach, and C. Bayan Bruss. Latent-CF: A Simple

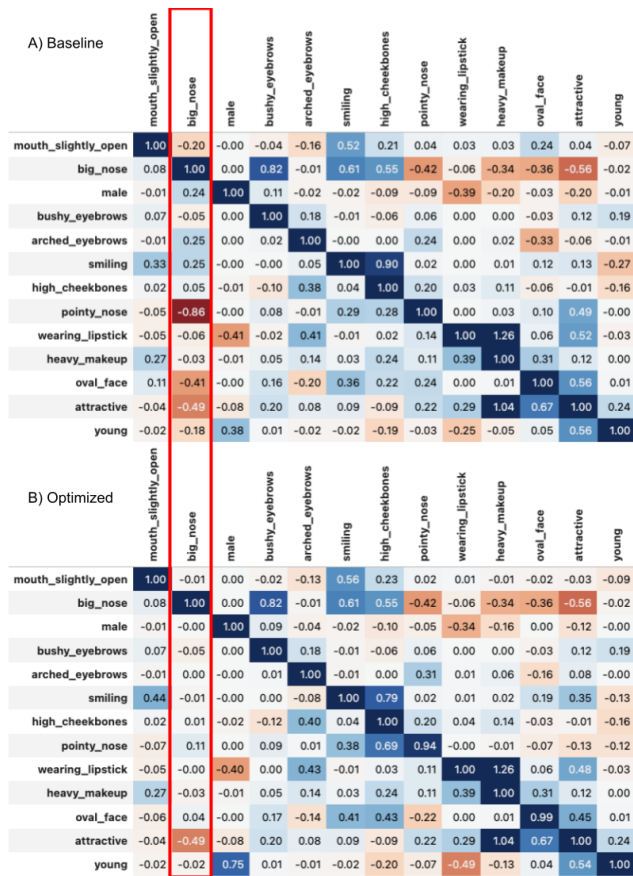


Figure 8. CF alignment matrices before and after optimization to remove the bias for *big_nose* on a hold out test set. The figure shows a dramatic reduction in relative change for most classifiers and *big_nose* with limited residual impact on other relationships.

Baseline for Reverse Counterfactual Explanations. In *Neural Information Processing Systems (NeurIPS) Fair AI in Finance Workshop*, 2020. 1, 2

[4] Alejandro Barredo-Arrieta and Javier Del Ser. Plausible Counterfactuals: Auditing Deep Learning Classifiers with Realistic Adversarial Examples. In *International Joint Conference on Neural Networks*, 2020. 2

[5] Christian F. Baumgartner, Lisa M. Koch, Kerem Can Tezcan, Jia Xi Ang, and Ender Konukoglu. Visual Feature Attribution Using Wasserstein GANs. In *Computer Vision and Pattern Recognition*, 2018. 2

[6] Sara Beery, Grant Van Horn, and Pietro Perona. Recognition in Terra Incognita. In *European Conference on Computer Vision*, 2018. 1

[7] Pierre Chambon, Christian Bluethgen, Jean-Benoit Delbrouck, Rogier der Sluijs, Małgorzata Połacin, Juan Manuel Zambrano Chaves, Tanishq Mathew Abraham, Shivanshu Purohit, Curtis P Langlotz, and Akshay Chaudhari. RoentGen: Vision-Language Foundation Model for Chest X-ray Generation, 2022. 2

[8] Joseph Paul Cohen, Rupert Brooks, Sovann En, Evan

Zucker, Anuj Pareek, Matthew P. Lungren, and Akshay Chaudhari. Gifsplanation via Latent Shift: A Simple Autoencoder Approach to Counterfactual Generation for Chest X-rays. *Medical Imaging with Deep Learning*, 2021. 1, 2

[9] Patrick Esser, Robin Rombach, and Björn Ommer. Taming transformers for high-resolution image synthesis. In *Computer Vision and Pattern Recognition*, 2021. 2

[10] Robert Geirhos, Jörn-Henrik Jacobsen, Claudio Michaelis, Richard Zemel, Wieland Brendel, Matthias Bethge, and Felix A. Wichmann. Shortcut learning in deep neural networks. *Nature Machine Intelligence*, 2020. 1

[11] Kyle A. Hasenstab, Justin Huynh, Samira Masoudi, Guilherme M. Cunha, Michael Pazzani, and Albert Hsiao. Feature Interpretation Using Generative Adversarial Networks (FIGAN): A Framework for Visualizing a CNN’s Learned Features. *IEEE Access*, 2023. 2

[12] Shalmali Joshi, Oluwasanmi Koyejo, Been Kim, and Joydeep Ghosh. xGEMs: Generating Exemplars to Explain Black-Box Models, 2018. 1, 2

[13] Tero Karras, Samuli Laine, and Timo Aila. A Style-Based Generator Architecture for Generative Adversarial Networks. In *Transactions on Pattern Analysis and Machine Intelligence*, 2021. 2

[14] Been Kim, Martin Wattenberg, Justin Gilmer, Carrie Cai, James Wexler, Fernanda Viegas, and Rory Sayres. Interpretability beyond feature attribution: Quantitative Testing with Concept Activation Vectors (TCAV). In *International Conference on Machine Learning*, 2018. 2

[15] Narine Kokhlikyan, Vivek Miglani, Miguel Martin, Edward Wang, Bilal Alsallakh, Jonathan Reynolds, Alexander Melnikov, Natalia Kliushkina, Carlos Araya, Siqi Yan, and Orion Reblitz-Richardson. Captum: A unified and generic model interpretability library for PyTorch, 2020. 3

[16] David Krueger, Ethan Caballero, Joern Henrik Jacobsen, Amy Zhang, Jonathan Binas, Dinghuai Zhang, Remi Le Priol, and Aaron Courville. Out-of-Distribution Generalization via Risk Extrapolation. In *International Conference of Machine Learning*, 2021. 5

[17] Ziwei Liu, Ping Luo, Xiaogang Wang, and Xiaoou Tang. Deep learning face attributes in the wild. In *International Conference on Computer Vision*, 2015. 2

[18] Mehdi Mirza and Simon Osindero. Conditional Generative Adversarial Nets, 2014. 2

[19] Jose G. Moreno-Torres, Troy Raeder, Rocío Alaiz-Rodríguez, Nitesh V. Chawla, and Francisco Herrera. A unifying view on dataset shift in classification. *Pattern Recognition*, 2012. 1

[20] Chris Olah, Alexander Mordvintsev, and Ludwig Schubert. Feature Visualization. *Distill*, 2017. 2

[21] Chris Olah, Nick Cammarata, Ludwig Schubert, Gabriel Goh, Michael Petrov, and Shan Carter. Zoom In: An Introduction to Circuits. *Distill*, 2020. 2

[22] Adam Paszke, Sam Gross, Francisco Massa, Adam Lerer, James Bradbury, Gregory Chanan, Trevor Killeen, Zeming Lin, Natalia Gimelshein, Luca Antiga, Alban Desmaison, Andreas Köpf, Edward Yang, Zach DeVito, Martin Raison, Alykhan Tejani, Sasank Chilamkurthy, Benoit Steiner, Lu

- Fang, Junjie Bai, and Soumith Chintala. PyTorch: An Imperative Style, High-Performance Deep Learning Library. *Neural Information Processing Systems*, 2019. 3
- [23] Marco Tulio Ribeiro, Sameer Singh, and Carlos Guestrin. "Why Should I Trust You?": Explaining the Predictions of Any Classifier. 2016. 2
- [24] Laura Rieger, Chandan Singh, W. James Murdoch, and Bin Yu. Interpretations are useful: Penalizing explanations to align neural networks with prior knowledge. In *International Conference on Machine Learning*, 2020. 5
- [25] Andrew Ross, Michael C Hughes, and Finale Doshi-Velez. Right for the Right Reasons: Training Differentiable Models by Constraining their Explanations. In *International Joint Conference on Artificial Intelligence*, 2017. 1
- [26] Shiori Sagawa, Pang Wei Koh, Tatsunori B. Hashimoto, and Percy Liang. Distributionally Robust Neural Networks for Group Shifts: On the Importance of Regularization for Worst-Case Generalization. *International Conference on Learning Representations*, 2020. 5
- [27] Pouya Samangouei, Ardavan Saeedi, Liam Nakagawa, and Nathan Silberman. ExplainGAN: Model Explanation via Decision Boundary Crossing Transformations. In *European Conference on Computer Vision*, 2018. 2
- [28] Kathryn Schutte, Olivier Moindrot, Paul Hérent, Jean-Baptiste Schiratti, and Simon Jégou. Using StyleGAN for Visual Interpretability of Deep Learning Models on Medical Images. In *Medical Imaging meets NeurIPS*, 2020. 2
- [29] Jarrel C.Y. Seah, Jennifer S.N. Tang, Andy Kitchen, Frank Gaillard, and Andrew F. Dixon. Chest radiographs in congestive heart failure: Visualizing neural network learning. *Radiology*, 2019. 2
- [30] Karen Simonyan, Andrea Vedaldi, and Andrew Zisserman. Deep Inside Convolutional Networks: Visualising Image Classification Models and Saliency Maps. In *International Conference on Learning Representations (ICLR)*, 2014. 2
- [31] Sumedha Singla, Motahhare Eslami, Brian Pollack, Stephen Wallace, and Kayhan Batmanghelich. Explaining the black-box smoothly—A counterfactual approach. *Medical Image Analysis*, 2023. 2
- [32] Jost Tobias Springenberg, Alexey Dosovitskiy, Thomas Brox, and Martin Riedmiller. Striving for Simplicity: The All Convolutional Net. In *International Conference on Learning Representations Workshop*, 2015. 2, 5
- [33] Mukund Sundararajan, Ankur Taly, and Qiqi Yan. Axiomatic Attribution for Deep Networks. In *International Conference on Machine Learning*, 2017. 2, 5
- [34] Simon Vandenhende, Stamatios Georgoulis, Bert De Brabandere, and Luc Van Gool. Branched Multi-Task Networks: Deciding What Layers To Share. *British Machine Vision Conference*, 2020. 2
- [35] Sahil Verma, Varich Boonsanong, Minh Hoang, Keegan E. Hines, John P. Dickerson, and Chirag Shah. Counterfactual Explanations and Algorithmic Recourses for Machine Learning: A Review. In *Neural Information Processing Systems (NeurIPS) Retrospectives Workshop*, 2020. 1, 2, 6
- [36] Mitchell Wortsman, Gabriel Ilharco, Samir Yitzhak Gadre, Rebecca Roelofs, Raphael Gontijo-Lopes, Ari S. Morcos, Hongseok Namkoong, Ali Farhadi, Yair Carmon, Simon Kornblith, and Ludwig Schmidt. Model soups: averaging weights of multiple fine-tuned models improves accuracy without increasing inference time. In *International Conference on Machine Learning*, 2022. 5
- [37] Huimin Zeng, Zhenrui Yue, Ziyi Kou, Yang Zhang, Lanyu Shang, and Dong Wang. Fairness-aware training of face attribute classifiers via adversarial robustness. *Knowledge-Based Systems*, 2023. 5

Identifying Spurious Correlations using Counterfactual Alignment

Supplementary Material

8. Appendix

	blurry	gray_hair	bald	wearing_hat	male	sideburns	wearing_necktie	mustache	chubby	big_nose	double_chin	receding_hairline	goatee	narrow_eyes	bags_under_eyes	eyeglasses	big_lips	black_hair	no_beard	smiling	mouth_slightly_open	high_cheekbones	wearing_earrings	wearing_necklace	wavy_hair	pointy_nose	blond_hair	bangs	heavy_makeup	wearing_lipstick	rosy_cheeks	arched_eyebrows	oval_face	attractive	pale_skin	young	straight_hair	bushy_eyebrows	5_o_clock_shadow	brown_hair	
blurry	1.00	0.01	0.00	-0.16	0.15	-0.12	-0.01	0.04	-0.02	-0.18	0.02	0.01	-0.10	0.05	-0.13	-0.04	-0.08	-0.02	0.08	-0.09	-0.03	-0.05	-0.01	-0.06	-0.03	-0.07	0.04	-0.03	-0.07	-0.25	-0.02	-0.12	-0.01	-0.19	-0.10	-0.10	0.00	-0.00	-0.07	0.02	-0.05
gray_hair	-0.00	1.00	-0.05	-0.03	0.04	-0.02	0.11	0.07	-0.05	0.14	0.03	0.31	-0.00	-0.04	0.15	0.01	-0.07	-0.01	0.06	-0.04	-0.04	-0.05	-0.03	0.00	0.02	0.03	-0.22	-0.06	-0.07	-0.05	-0.00	-0.11	-0.11	-0.09	-0.00	-0.24	-0.04	-0.07	-0.18	-0.03	
bald	-0.00	-0.12	1.00	-0.05	0.02	0.04	0.04	-0.01	0.12	0.07	0.09	-0.23	0.21	0.00	0.06	-0.02	-0.00	-0.05	-0.10	-0.00	-0.07	-0.01	-0.01	-0.01	0.02	-0.02	-0.01	-0.01	-0.01	-0.00	0.05	0.05	-0.02	-0.00	-0.05	-0.10	0.04	0.01	-0.02		
wearing_hat	0.00	-0.01	-0.06	1.00	0.09	0.04	0.01	-0.02	0.07	0.12	0.08	-0.04	0.00	-0.07	0.19	0.00	-0.13	-0.39	-0.00	-0.03	-0.03	-0.07	-0.10	-0.04	-0.05	-0.01	-0.01	-0.03	-0.09	-0.11	-0.01	-0.19	-0.08	-0.10	-0.02	-0.22	-0.16	-0.05	0.06	-0.00	
male	-0.00	0.05	0.08	0.02	1.00	0.07	0.10	0.06	0.04	0.19	0.09	-0.01	0.26	0.04	0.23	-0.01	-0.07	-0.04	-0.65	-0.05	-0.07	-0.11	-0.31	-0.12	-0.03	-0.05	-0.06	-0.05	-0.51	-0.69	-0.05	-0.21	-0.15	-0.16	-0.04	-0.10	0.05	0.09	0.36	0.03	
sideburns	-0.00	-0.01	0.00	0.02	1.00	0.01	0.01	0.12	0.01	-0.06	-0.06	0.11	0.01	0.06	-0.00	-0.09	-0.03	-0.18	-0.03	-0.11	-0.09	-0.07	-0.01	0.00	-0.03	-0.01	-0.00	-0.02	-0.02	0.00	-0.08	-0.02	0.01	-0.01	-0.08	0.01	-0.05	-0.04	0.04		
wearing_necktie	-0.00	0.04	0.04	-0.00	0.01	0.02	1.00	0.03	0.12	0.10	0.14	0.05	0.03	0.03	0.13	0.01	-0.02	-0.03	-0.00	-0.00	-0.03	-0.03	-0.02	-0.02	-0.03	0.01	-0.01	-0.00	-0.01	-0.01	0.01	-0.06	-0.06	-0.01	-0.01	-0.10	0.06	0.04	0.00	-0.01	
mustache	0.00	0.01	-0.05	-0.01	0.01	-0.17	0.07	1.00	0.04	0.18	0.10	0.12	0.31	0.12	0.09	-0.00	0.14	0.12	-0.20	-0.09	-0.32	-0.00	0.05	0.05	-0.02	-0.04	-0.01	-0.00	-0.02	-0.02	0.01	0.05	-0.03	-0.03	-0.00	-0.12	0.01	0.13	-0.14	-0.05	
chubby	0.00	0.02	0.06	0.01	0.01	0.11	0.11	0.05	1.00	0.28	0.64	0.04	0.01	0.08	0.10	0.00	0.06	0.04	-0.09	-0.02	-0.02	0.04	0.00	0.01	0.03	-0.23	-0.01	-0.00	0.01	-0.01	0.01	-0.13	-0.00	-0.22	-0.00	-0.30	-0.10	-0.08	0.02	-0.03	
big_nose	-0.01	0.06	0.06	0.03	0.06	-0.05	0.05	0.13	0.27	1.00	0.30	0.13	0.14	0.05	0.63	0.01	0.19	0.04	-0.03	0.08	0.05	0.18	0.12	0.09	0.03	-0.36	-0.04	-0.03	-0.08	-0.06	0.01	0.05	-0.20	-0.42	-0.01	-0.37	-0.10	0.08	-0.02	-0.09	
double_chin	-0.00	0.09	0.09	0.00	0.06	-0.09	0.10	0.05	0.69	0.40	1.00	0.10	-0.07	0.08	0.25	0.02	0.04	-0.01	0.21	0.19	0.09	0.21	-0.02	0.01	0.03	-0.17	-0.02	-0.01	-0.05	-0.05	0.04	-0.13	-0.09	-0.09	-0.08	-0.37	-0.15	-0.08	-0.15	-0.03	
receding_hairline	-0.00	-0.15	-0.04	-0.01	-0.04	-0.14	0.02	0.03	0.08	0.18	0.11	1.00	-0.02	0.02	0.08	-0.01	0.04	0.08	0.21	-0.01	0.03	0.04	0.06	0.02	0.01	0.00	-0.02	-0.00	-0.02	0.01	-0.04	-0.07	-0.14	-0.25	-0.00	-0.22	-0.17	-0.15	-0.26	-0.07	
goatee	-0.00	-0.02	0.07	-0.00	0.02	-0.11	0.01	0.20	0.02	0.12	0.02	0.03	1.00	0.01	0.00	-0.00	0.08	0.00	-0.15	0.08	0.08	0.06	-0.00	0.01	-0.03	-0.10	-0.01	0.02	-0.00	-0.00	0.00	-0.02	-0.07	-0.00	-0.00	-0.03	-0.01	-0.06	-0.35	-0.02	
narrow_eyes	-0.00	-0.01	-0.00	-0.01	0.01	0.01	0.01	0.04	0.07	0.04	0.04	0.01	1.00	0.11	-0.05	0.00	0.00	0.06	0.08	0.05	0.02	0.01	0.01	-0.01	-0.06	-0.01	0.00	-0.12	-0.08	-0.03	-0.08	-0.15	-0.08	-0.01	-0.04	0.05	0.06	0.00	0.02		
bags_under_eyes	-0.00	0.00	0.06	0.02	0.02	0.03	0.06	0.01	0.08	0.51	0.11	0.07	0.00	-0.01	1.00	-0.07	-0.00	0.07	0.03	0.06	0.02	0.18	0.00	-0.01	-0.08	0.02	-0.04	-0.01	-0.13	-0.04	-0.05	-0.02	-0.32	-0.34	-0.01	-0.39	0.02	0.04	-0.03	0.02	
eyeglasses	-0.00	0.02	0.01	0.00	-0.00	-0.02	0.02	0.00	0.03	0.10	0.04	0.02	0.04	-0.05	-0.01	1.00	-0.04	-0.02	0.03	0.02	0.06	0.02	-0.01	-0.00	-0.01	-0.01	0.00	-0.02	-0.03	-0.02	-0.00	-0.05	-0.00	-0.02	-0.01	-0.12	0.01	-0.01	-0.05	0.00	
big_lips	-0.00	-0.02	-0.01	0.02	-0.02	-0.11	-0.01	0.02	0.06	0.31	0.05	0.04	0.02	0.03	0.00	-0.00	1.00	0.22	-0.01	0.06	0.25	0.09	0.28	0.17	0.09	-0.12	-0.07	0.01	0.31	0.17	-0.03	0.27	-0.18	-0.00	0.04	0.25	-0.09	0.12	0.00	-0.06	
black_hair	-0.00	-0.00	-0.03	-0.01	-0.00	-0.02	-0.00	0.02	0.03	0.09	-0.00	0.02	0.01	0.00	-0.03	-0.00	0.12	1.00	0.02	-0.04	0.05	-0.03	0.00	-0.04	-0.08	-0.00	-0.01	0.02	0.02	-0.05	0.09	-0.05	-0.01	-0.02	0.11	0.06	0.11	-0.01	-0.19		
no_beard	0.01	0.03	-0.01	-0.00	-0.06	-0.26	0.04	-0.04	0.04	0.01	0.08	0.00	-0.19	-0.00	0.01	-0.00	-0.02	0.02	1.00	0.11	0.06	0.13	0.02	-0.01	-0.01	0.00	0.01	0.00	0.02	0.06	0.00	0.06	0.02	0.01	-0.04	0.04	0.03	-0.61	-0.02		
smiling	-0.00	0.01	0.01	-0.00	-0.01	-0.03	0.01	0.01	-0.03	0.11	0.06	-0.03	0.03	0.02	0.14	0.01	0.04	-0.01	0.01	1.00	0.26	0.63	-0.01	0.04	-0.00	0.08	0.02	0.01	0.09	0.04	0.19	0.07	0.12	0.15	-0.00	-0.02	-0.01	-0.04	-0.01	-0.04	
mouth_slightly_open	0.00	0.00	-0.00	0.00	-0.00	-0.02	-0.01	-0.03	-0.03	-0.01	-0.01	-0.01	-0.03	0.05	0.06	-0.01	0.02	-0.01	0.08	0.39	1.00	0.29	-0.04	-0.02	-0.03	0.03	0.01	0.00	-0.01	0.00	0.05	-0.02	-0.04	-0.03	-0.02	-0.01	0.02	-0.16	-0.06	-0.02	
high_cheekbones	-0.00	0.00	0.00	-0.01	-0.08	-0.02	-0.01	-0.01	0.00	0.16	0.04	0.01	-0.01	0.02	0.21	-0.00	0.00	0.02	0.10	0.63	0.17	1.00	0.15	0.04	0.05	0.07	0.01	0.01	0.10	0.10	0.26	0.19	0.05	0.00	-0.06	-0.10	-0.05	-0.06	-0.08	-0.03	
wearing_earrings	-0.00	0.00	-0.00	-0.01	-0.11	0.00	-0.02	0.00	0.01	0.06	0.01	0.06	-0.00	0.02	-0.03	-0.01	0.10	0.01	0.01	0.05	0.06	0.13	1.00	0.07	0.00	0.06	-0.00	0.00	0.20	0.14	0.13	0.18	-0.06	-0.01	-0.01	-0.02	-0.06	-0.05	-0.01	-0.02	
wearing_necklace	-0.00	0.01	0.00	-0.00	-0.01	-0.00	-0.01	-0.00	0.02	0.35	0.13	0.02	-0.00	0.01	0.29	-0.00	0.18	-0.00	0.00	0.05	0.04	0.09	1.00	0.05	0.07	0.00	0.00	0.05	0.07	0.12	0.24	-0.47	-0.39	-0.06	-0.23	-0.07	-0.11	-0.00	-0.07		
wavy_hair	0.00	0.00	-0.01	-0.01	-0.00	0.00	-0.00	0.00	0.01	0.01	0.01	-0.02	-0.00	0.01	-0.03	0.00	0.04	-0.03	-0.00	0.03	0.02	0.05	0.01	-0.01	-1.00	-0.00	-0.00	0.00	0.11	0.04	0.05	0.07	0.03	0.06	0.00	-0.03	-0.71	-0.02	0.00	0.11	
pointy_nose	0.00	0.01	0.00	-0.01	-0.09	-0.02	0.00	-0.01	-0.22	-0.47	-0.10	-0.05	-0.06	-0.04	-0.13	-0.00	-0.09	-0.07	0.05	0.24	0.13	0.25	0.12	0.02	-0.03	1.00	0.07	-0.00	0.28	0.17	0.36	0.27	0.05	0.34	-0.03	-0.04	-0.01	0.09	0.02	0.00	
blond_hair	-0.00	-0.03	-0.01	-0.01	-0.10	-0.01	-0.01	-0.00	-0.03	-0.28	-0.07	-0.11	-0.02	-0.04	-0.18	-0.02	-0.07	-0.01	0.02	0.05	-0.03	0.06	0.01	0.05	0.04	0.15	1.00	0.05	0.31	0.21	0.09	0.10	0.25	0.35	0.01	0.20	0.03	-0.13	-0.01	-0.20	
bangs	-0.00	-0.01	-0.00	-0.07	-0.09	-0.02	-0.00	-0.00	-0.03	-0.05	-0.04	-0.00	0.00	0.00	-0.02	-0.00	0.05	0.03	0.03	0.11	0.00	0.15	0.03	0.05	-0.06	0.04	0.07	1.00	0.21	0.17	0.09	-0.01	0.17	0.23	-0.00	0.06	0.04	-0.02	-0.06	-0.02	
heavy_makeup	0.00	-0.00	-0.00	-0.07	0.00	-0.00	-0.00	-0.01	-0.20	-0.04	-0.03	-0.00	-0.04	-0.32	-0.00	0.13	0.01	0.00	0.08	0.17	0.11	0.26	0.01	0.11	0.10	0.03	0.02	1.00	0.36	0.24	0.31	0.34	0.45	0.03	0.15	-					

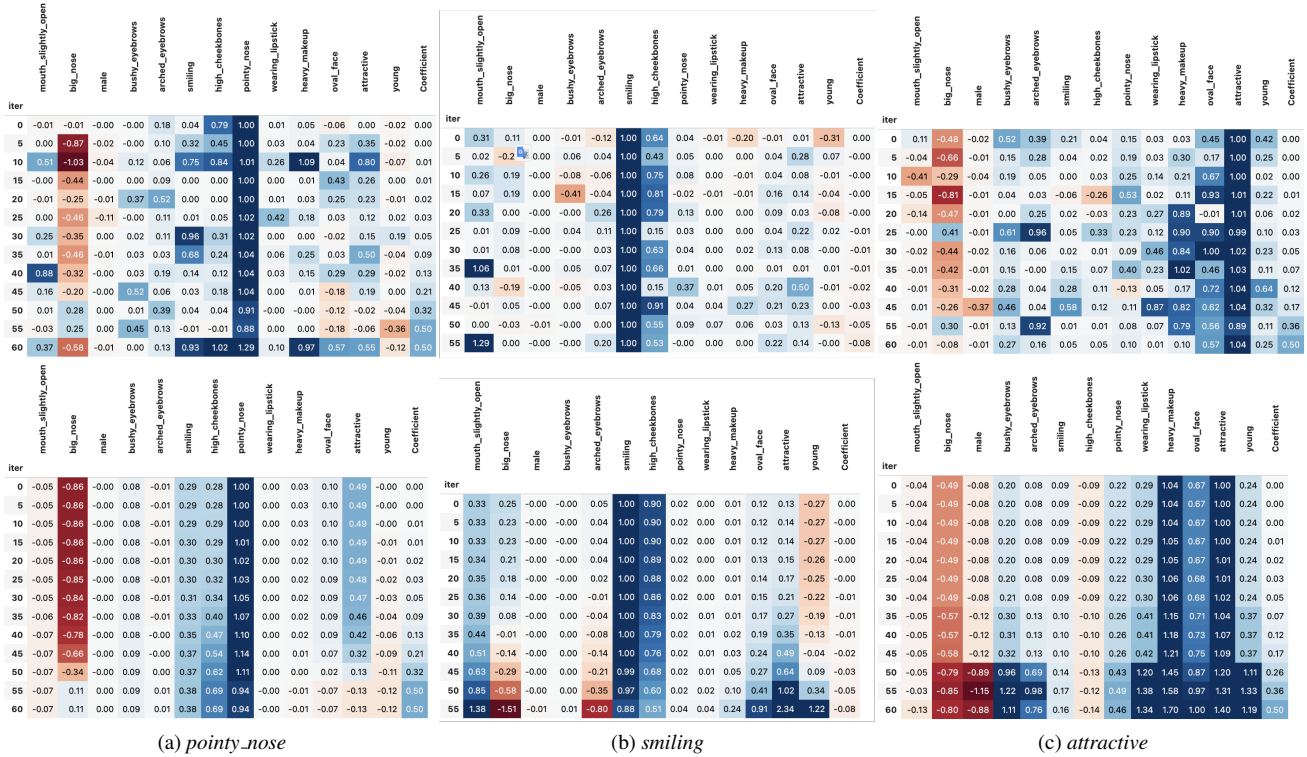


Figure 10. Visualization of the training from §4.5 reducing the bias of *big_nose*. The model being evaluated is $f'_{target}(x) = f_{target}(x) + \beta f_{big_nose}(x)$ where β is specified by the coefficient column. The metric here is relative change computed between the $f'_{target}(x)$, where *target* is specified in the caption, and the classifier specified by the column header. The top row is from the training set performed on batches (which explains the variance) and the second row is the results on the entire validation set. The row of each table is for a specific iteration. The iterations proceed downward. The training of *attractive* shown here does not result in a debiased model, the relative change diverges from 0 indicating a failed training.